Supplementary Information

Enhancing Efficiency in Organic Electronics via J-Aggregation Modulation with Non-Halogenated Solvents

Guangting Cai [1], Zhenmin Zhao [1]*, Sein Chung [2], Liang Bai [1], Lixing Tan [1], Xin Li [1], Jingjing Zhao [1], Yuan Liu [1], Kilwon Cho [2], Zhipeng Kan [1,3]

[1] Center on Nanoenergy Research, Institute of Science and Technology for Carbon Peak & Neutrality, School of Physical Science & Technology, Guangxi University, Nanning 530004, China.

[2] Department of Chemical Engineering, Pohang University of Science and Technology, Pohang 37673, South Korea.

[3] State Key Laboratory of Featured Metal Materials and Life-cycle Safety for Composite Structures, Nanning 530004, China.

* Corresponding author, E-mail: 2007401038@st.gxu.edu.cn

Content

1. Experimental Section/Methods

Materials: PM6, GS-ISO and PFNBr were purchased from Solarmer, Inc (Beijing). All materials were used as received without further purification.

Device Fabrication: Organic solar cells (OSCs) were fabricated using a conventional device configuration of ITO/PEDOT :PSS/active layers/PFNBr/Al. The glass substrates were coated with a layer of indium tin oxide (ITO, 15 Ω/sq) (device area: 0.04 cm2). The substrates were prewashed with isopropanol to remove organic residues before being immersed in an ultrasonic bath of soap for 15 minutes. The samples were rinsed in flowing deionized water for 5 minutes, followed by sonication for 15 minutes each in successive baths of deionized water, acetone, and isopropanol. Next, the samples were dried with pressurized nitrogen and then exposed to UV-ozone plasma for 15 minutes. A thin layer of PEDOT :PSS (~30 nm) (CLEVIOSTM P VP AI 4083, Heraeus, Germany) was spin-coated onto the UV-treated substrates. The PEDOT-coated substrates were subsequently annealed on a hot plate at 150 °C for 20 minutes and then transferred into a glovebox for active layer deposition. All active layer solutions were prepared in a nitrogen-filled glovebox using the polymer donor (PM6) and small molecule acceptor (GS-ISO). The solvents used were untreated CF, O-XY, and O-XY with DIO additive. For the O-XY+DIO solution system, 1,8-diiodooctane (DIO) was first dissolved in o-xylene and stirred at room temperature for 1 hour before being used for active layer solution preparation. The active layer solutions of PM6:GS-ISO (1:1.3, 16 mg/mL in chloroform), PM6:GS-ISO (1:1.3, 25 mg/mL in o-xylene), and PM6:GS-ISO (1:1.3, 25 mg/mL in o-xylene with 0.5% vol 1,8-diiodooctane (DIO)) were stirred for 3 hours. The blend solutions were then directly spin-coated at 4000 rpm onto PEDOT:PSS ITO substrates, followed by thermal annealing at 160°C for 25 minutes. A PFNBr layer was then spin-coated onto the active layer as an electron transport layer. The substrates were then pumped down in high vacuum at a pressure of 2×10^{-6} Torr, and an Al layer (100 nm) was thermally evaporated onto the active layer.

2. J-V under indoor light and AM 1.5G

Table S1. Device parameters of PM6:GS-ISO BHJ devices in different solvent systems under indoor light (2700 K, 1000 lux). The values are averaged from 15 devices.

Active layer	V_{OC}[V]	J_{SC}[μA/cm^2]	FF[%]	PCE[%]
PM6:GS-ISO	1.06	102.3	71.83	25.61
(CF)	(1.06±0.002)	(100.6±0.34)	(71.42±0.48)	(24.35±0.67)
PM6:GS-ISO	1.08	104.8	69.76	25.84
(O-XY)	(1.08±0.002)	(103.6±0.30)	(68.63±0.54)	(24.65±0.58)
PM6:GS-ISO	1.08	102.8	71.70	26.56
(O-XY+DIO)	(1.08±0.003)	(102.1±0.42)	(71.09±0.48)	(25.85±0.35)

Table S2. Device parameters of PM6:GS-ISO BHJ devices in different solvent systems under AM 1.5G. The values are averaged from 15 devices.

Active layer	V_{OC}[V]	J_{SC}[mA/cm^2]	FF[%]	PCE[%]
PM6:GS-ISO	1.22	11.44	70.46	9.87
(CF)	(1.22±0.005)	(11.24±0.58)	(70.06±0.49)	(9.42±0.41)
PM6:GS-ISO	1.21	11.51	67.64	9.39
(O-XY)	(1.21±0.002)	(11.47±0.50)	(67.98±0.56)	(9.13±0.23)
PM6:GS-ISO	1.21	11.69	70.27	9.97
(O-XY+DIO)	(1.21±0.005)	(11.34±0.67)	(69.32±0.45)	(9.49±0.43)

3. PL measurement

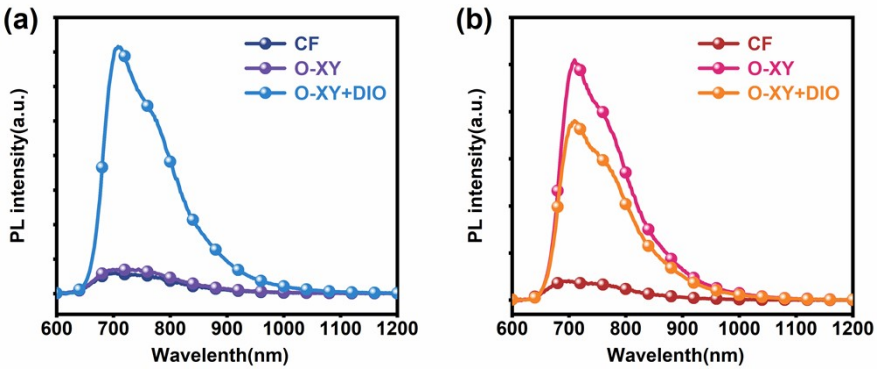

Figure. S1 PL spectra of **a)** PM6, **b)** GS-ISO processed with different solvents.

4. Absorption under indoor light

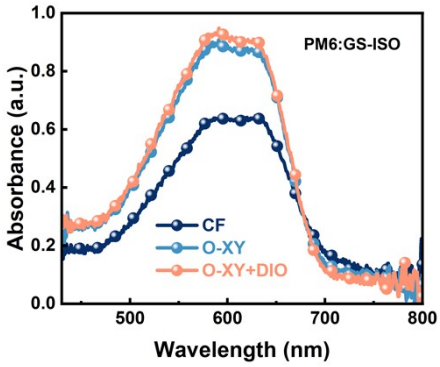

Figure. S2 absorption spectra of PM6: GS-ISO processed with different solvents.

5. Contact Angle

The contact angles were performed on a L2004A1 (Ossila England) contact angle meter. Then the surface free energy was calculated by Owens-Wendt method [1, 2]:

$$\varepsilon_L \times (1+\cos\theta) = 2 \times (\varepsilon_L^d \cdot \epsilon_{sv}^d)^{1/2} + 2 \times (\varepsilon_L^p \cdot \varepsilon_{sv}^p)^{1/2}$$

where ε_L and ε_S are the surface free energy of the probe liquid and sample, respectively, and θ is the contact angle of samples. The average contact angles of two liquids (deionized water and formamide) were measured and the results (dynamic analysis by video) in **Figure S1**, and the average contact angles and surface energy parameters are summarized in **Table S2**. Then calculate the Flory-Huggins interaction parameter $\chi_{donor-acceptor}$ for the blend to show the binary miscibility from:

$$K(\chi_{donor}^{1/2} - \chi_{acceptor}^{1/2})^2$$

where χ is the surface energy of the material, K is the proportionality constant.

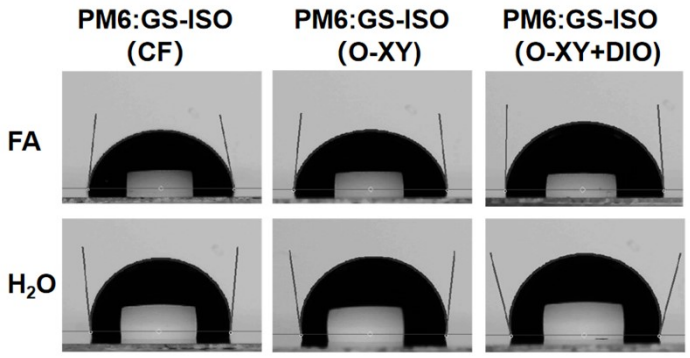

Figure S3. The contact angles of the films in deionized formamide (FA) and water (H_2O).

Table S3. Summarized contact angles of the materials.

Films	Contact angle (deg)		Surface free energy (mJm^{-2})
	FA	H_2O	
PM6:GS-ISO (CF)	77.15	100.77	26.71
PM6:GS-ISO (O-XY)	84.32	96.72	17.63
PM6:GS-ISO (O-XY+DIO)	87.62	104.08	17.16

6. GIWAXS measurements of PM6:GS-ISO with and without additives

Grazing-incidence wide-angle X-ray scattering (GIWAXS) was carried out to investigate the molecular packing and molecular orientation in the thin films. The π–π stacking distance (d-spacing) and crystalline coherence length (CCL) were calculated quantitatively using the equations d-spacing = 2π/q and CCL = 2πK/Δq, where q, Δq and the K constant represent the peak positions, full width at half maximum. [3, 4]

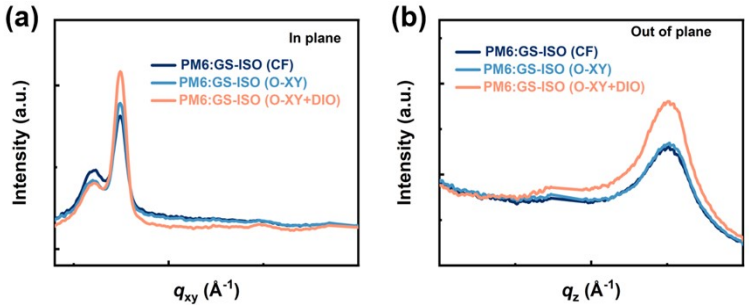

Figure S4. In-plane (dash lines) and out-of-plane (solid lines) line cuts of PM6:GS-ISO films cast from a) CF, b) O-XY, c) O-XY with DIO.

Table S4. Out-of-plane parameters; peak location, d-spacing, FWHM, and crystal coherence length (CCL) extracted from the 2D GIWAXS of PM6:GS-ISO films with and without additives.

Component	Peak	Peak position (Å^{-1})	d-spacing (Å)	FWHM (Å^{-1})	CCL (Å)
PM6:GS-ISO (CF)	OOP(010)	1.67	3.76	0.14	40.39
		1.73	3.63	0.09	62.83
PM6:GS-ISO (O-XY)	OOP(010)	1.69	3.72	0.10	56.55
		1.76	3.57	0.07	80.78
PM6:GS-ISO (O-XY+DIO)	OOP(010)	1.70	3.69	0.06	94.25
		1.75	3.58	0.07	80.78

Table S5. In-plane parameters; peak location, d-spacing, FWHM, and crystal coherence length (CCL) extracted from the 2D GIWAXS of PM6:GS-ISO films with and without additives.

Component	Peak	Peak position ($Å^{-1}$)	d-spacing (Å)	FWHM ($Å^{-1}$)	CCL (Å)
PM6:GS-ISO (CF)	IP (001)	0.37	16.98	0.041	137.92
PM6:GS-ISO (O-XY)	IP (001)	0.37	16.98	0.039	144.99
PM6:GS-ISO (O-XY+DIO)	IP (001)	0.37	16.98	0.034	166.32

7. SCLC Measurements

The carrier mobility (hole and electron mobility) of the photoactive layer was determined by fitting the dark current of hole/electron-only diodes to the space-charge-limited current (SCLC) model. Electron-only and hole-only devices were fabricated for the J−V measurements. The structure of the electron-only device was ITO/ZnO/BHJ/ZnO/Al and the hole-only was ITO/PEDOT:PSS/BHJ/MoO3/Al.[1] The single-carrier device was connected to a Source Measure Unit (Keithley, Model 236 SMU) which provides DC voltage to the electron-only devices. The J−V values of different DC voltages can be detected and recorded through SMU. The J-V characteristics were further analyzed by the space-charge-limited-current (SCLC) method to extract zero-field carrier mobilities, where SCLC is described by [5, 6]:

$$J = \frac{9\varepsilon_0\varepsilon_\gamma\mu_0 V^2}{8\mathrm{L}^3}\exp\left(0.89\beta\sqrt{\frac{\mathrm{V}}{\mathrm{L}}}\right)$$

where J is the current density, L is the film thickness of the active layer, μ0 is the hole or electron mobility, εr is the relative dielectric constant of the transport medium, ε0 is the permittivity of free space (8.85 $\times10^{-12}$ F m^{-1}), V (= V_{appl} - V_{bi}) is the internal voltage in the device, where V_{appl} is the applied voltage to the device and V_{bi} is the built-in voltage due to the relative work function difference of the two electrodes. **Table S1**. Summarized μe and μh treated under different conditions.

Table S6. Summarized μ_e and μ_h under different conditions.

Photoactive layer	μ_e($cm^2V^{-1}s^{-1}$)	μ_h($cm^2V^{-1}s^{-1}$)	μ_e/μ_h
PM6:GS-ISO (CF)	1.42×10^{-4}	1.65×10^{-4}	1.16
PM6:GS-ISO (O-XY)	1.35×10^{-4}	1.22×10^{-4}	1.11
PM6:GS-ISO (O-XY+DIO)	1.93×10^{-4}	1.82×10^{-4}	1.06

8. DLTS Measurements

Deep level transient spectroscopy was simulated current-based. The transient current response is analyzed by applying a negative pressure from -1V to -3V to the device in the dark. The transient current reaches its maximum response at t=0.1s regardless of the bias voltage, and the peak rises gradually at 0.1s with the increase of the bias voltage. Apart from the displacement current generated by the circuit, there is also the current emitted by the discrete energy trap. Using the following equation to estimate the defect distributions in organic semiconductors. Considering the dependence of carrier transport position in the device, the current peak in the first 0.1μs is mainly caused by the displacement current, so the fitting of 0.1 ~ 100μs at room temperature are dominant. The trapped defect state volume density N_t of the discrete energy trap can be expressed as [7, 8]:

$$j_{te}(t) = \frac{1}{\tau_{te}} \cdot q \cdot d \cdot N_t \cdot \exp\left(-\frac{t}{\tau_{te}}\right)$$

Where $j_{te}(t)$ is trap emission current, τ_{te} is catch-trap emission time constant, q is a single charge amount, d is the membrane thickness of the device, N_t is the trap state density.

9. References

[1] Sun, Y. et al. Suppressing nongeminate recombination with two well-compatible polymer donors enables 16.6% efficiency all-polymer solar cells. *Chem. Eng. J.* 2023, **470,** 144186.

[2] Huang, X. et al. Triggering the Donor−Acceptor Phase Segregation with Solid Additives Enables 16.5% Efficiency in All-Polymer Solar Cells. *ACS Appl. Mater. Interfaces.* 2023, **15,** 44012−44021.

[3] Qin, Y. et al. Low Temperature Aggregation Transitions in N3 and Y6 Acceptors Enable Double-Annealing Method That Yields Hierarchical Morphology and Superior Efficiency in Nonfullerene Organic Solar Cells. *Adv. Funct. Mater.* 2020, **30,** 2005011.

[4] Sun, R. et al. A Layer-by-Layer Architecture for Printable Organic Solar Cells Overcoming the Scaling Lag of Module Efficiency. *Joule.* 2020, **4,** 407-419.

[5] Lv, J. et al. Phase separation and domain crystallinity control enable open-air-printable highly efficient and sustainable organic photovoltaics. *InfoMat.* 2024, **6,** e12530.

[6] Hu, D. et al. 15.34% efficiency all-small-molecule organic solar cells with an improved fill factor enabled by a fullerene additive. *Energy Environ. Sci.* 2020, **13,** 2134-2141

[7] Bozyigit, D., Jakob, M., Yarema, O., Wood, V. Deep level transient spectroscopy (DLTS) on colloidal-synthesized nanocrystal solids. *ACS Appl. Mater. Interfaces.* 2013, **5(8),** 2915−2919.

[8] Li, R., Li, B., Fang, X., Wang, D., Shi, Y., Liu, X., Chen, R., Wei, Z. Phase transition induced recrystallization and low surface potential barrier leading to 10.91%-efficient CsPbBr3 perovskite solar cells. *Adv. Mater.* 2021, **33(21),** 2100466.